Electrochimica Acta 139 (2014) 76–81

Contents lists available at ScienceDirect

Electrochimica Acta

journal homepage: www.elsevier.com/locate/electacta

Facile route for synthesis of mesoporous Cr_2O_3 sheet as anode materials for Li-ion batteries

Zhiqin Cao[a,b], Mingli Qin[a,*], Baorui Jia[a], Lin Zhang[a], Qi Wan[a], Mingshan Wang[a], Alex A. Volinsky[c], Xuanhui Qu[a]

[a] School of Materials Science and Engineering, University of Science and Technology Beijing, Beijing 100083, China
[b] School of Resources and Environmental Engineering, Pan Zhihua University, Pan Zhihua 617000, China
[c] Department of Mechanical Engineering, University of South Florida, Tampa FL 33620, USA

ARTICLE INFO

Article history:
Received 12 March 2014
Received in revised form 21 June 2014
Accepted 21 June 2014
Available online 11 July 2014

Keywords:
Solution combustion synthesis
Cr_2O_3
Lithium-ion batteries
Anode

ABSTRACT

Mesoporous Cr_2O_3 with a high specific surface area of 162 $m^2\ g^{-1}$ is prepared by the solution combustion method. The mesoporous Cr_2O_3 has a sheet structure, which consists of nanoparticles with an average size of 20 nm. As an anode electrode material for rechargeable lithium-ion batteries, the mesoporous Cr_2O_3 nanoparticles display enhanced electrochemical performance. Stable and reversible capacity of 480 mA h g^{-1} after 55 cycles is demonstrated. The enhanced electrochemical performance of the Cr_2O_3 can be attributed to the high surface area and morphological characteristics of mesoporous materials.

1. Introduction

Tremendous efforts are devoted to develop renewable energy sources to address multiple economic issues related to the exponential growth in global energy, consumption, rapid depletion of fossil fuels, increasing greenhouse gas emissions, and upward spike in the crude-oil and gasoline prices [1]. Lithium-ion batteries (LIBs), with high energy and power density are in great demand as energy sources for multiple applications, including hybrid electric vehicles and clean energy storage [2–5], which accelerates the search for new electrode materials with higher capacity and rate capabilities. Currently, graphite-based anodes are used in most commercially available rechargeable lithium-ion batteries, which can only provide a theoretical maximum capacity of about 372 mA h g^{-1}. Due to the low theoretical capacity, graphite electrodes can only supply relatively low energy storage ability, thus they cannot meet the increasing power demands. A new family of high energy anode materials beyond those based on lithium alloying/de-alloying, such as Sn, Si and several transition metal oxides, have been reported [6–13]. The lithium storage mechanism is the "conversion reaction", in which transition metal oxides, fluorides, oxyfluorides, sulfides, and nitrides react with lithium, leading to reversible in situ formation and decomposition of Li_yX (where X is O, S, F, or N), accompanying the reduction and oxidation of metal nanoparticles [14]. The reaction gives rise to high reversible capacity, ranging from 400 to 1100 mA h g^{-1} between 0.001 V and 3.0 V vs. Li/Li^+ [15–18].

Among various transition metal oxides that are prospective anodes for LIBs, Cr_2O_3 has been suggested as a promising candidate for anode electrode materials of the Li-ion battery due to its high theoretical specific lithium storage capacity (1058 mA h g^{-1}), relatively low lithium insertion potential among metal oxides (MO_x) and low cost [19–23]. However, the application of Cr_2O_3 is accompanied with a sharp capacity fade, which is considered to be caused by the huge volume variation, pulverization, electrical contact loss and formation of unstable solid electrolyte interphase (SEI) during the lithium ion insertion/extraction process. Mesoporous structure of Cr_2O_3 is expected to solve these problems. The mesoporous Cr_2O_3 materials have lots of advantages in the application of lithium batteries [24]. For example, the large surface area generated by mespores offers more active sites for the reactions (electronic and ionic transport). The small grain size of mesoporous materials allows fast completion of the lithium ion insertion/extraction to the small crystalline walls, thus improving the high-rate performance of lithium battery anodes due to a shorter diffusion length for lithium ion and electronic transport in nanoparticles.

Some methods have been reported for the preparation of mesoporous Cr_2O_3 materials, such as vacuum assisted impregnation and

* Corresponding author. Tel.: +86 10 82377286; fax: +86 10 62334311.
E-mail address: qinml@mater.ustb.edu.cn (M. Qin).

http://dx.doi.org/10.1016/j.electacta.2014.06.160
0013-4686/

nanocasting [24–26]. These methods rely on tedious processing or surfactants as templates for the synthesis of nanostructures. Hence, it is of significant interest to develop a facile, surfactant-free method to prepare mesoporous Cr_2O_3 nanocrystalline structure with high specific surface area. Solution combustion synthesis is a well known method for the preparation of nanocrystalline oxides [27–30]. This method has been regarded as one of the effective and economic methods due to its convenient processing, simple experimental setup, significant time saving and high purity products [31]. The method can prepare nanocrystalline products with high specific surface area due to a large volume of gases liberated during the combustion reaction [32]. In this work, we report the solution combustion synthesis method for the synthesis of mesoporous Cr_2O_3 with a high specific surface area directly from the reaction of metal nitrates-glycine. The as-prepared mesoporous Cr_2O_3 with high specific surface area exhibits excellent performance for lithium ion batteries.

2. Experimental

2.1. Synthesis

Cr_2O_3 nanoparticles were prepared by solution-combustion synthesis using chromium nitrate [$Cr(NO_3)_3{\cdot}9H_2O$] as the oxidant and glycine [NH_2CH_2COOH] as the fuel. Analytical reagent grade chemicals were purchased commercially. As a typical sample preparation procedure, $Cr(NO_3)_3{\cdot}9H_2O$ and NH_2CH_2COOH were dissolved in 150 mL deionized water under stirring to obtain a redox mixture. The mixture was filled in a 500 mL glass, and was heated in air on an electrical furnace whose temperature could be controlled. In this work, the temperature is controlled at 300°C. As heating continued, the solution evaporated and formed a gelatinous mass. It took about 5 minutes to form gelatinous mass. Upon further heating, the resultant mass swelled suddenly accompanied by the release of a lot of gases. The whole process of gel swelling and combustion appeared to undergo a self-propagating and non-explosive exothermic reaction, which took only several minutes, resulting in a fragile and foamy products.

2.2. Characterization and electrochemical measurements

The products were analyzed by X-ray diffractometer using Cu-K_α radiation (λ=0.1542 nm, Rigaku D/max-RB12). The morphology and particle size of products were observed by scanning electron microscopy (SEM, JSM-5600) and transmission electron microscopy (TEM, Tecnai G2 F30 S-TWIN). The specific surface area (SSA) was determined by the Brunauer-Emmett-Teller (BET) method using an automated surface area and pore size analyzer (QUADRASORB SI-MP, Quantachrome Instruments, Boynton Beach, FL).

Electrochemical measurements were performed in the CR2023-type coin cells. The Cr_2O_3 anode electrode (working electrode) was fabricated by mixing the active materials with acetylene black (AB) and a binder, poly(vinylidene fluoride) (PVDF), at weight ratios of 40:40:20. The mixture was dispersed in the NMP solvent to form slurry and uniformly pasted on the Cu foil with a blade. These prepared electrode sheets were dried at 120 °C in a vacuum oven for 12 h and pressed under a pressure of 200 kg m^{-2}. The CR2032-type coin cells were assembled in a glove box for electrochemical characterization. A non-aqueous solution of 1 M $LiPF_6$ in a 1:1 ethylene carbonate (EC) and dimethyl carbonate (DMC) was used as electrolyte. Li metal disk was used as the counter electrode for electrochemical testing. The cells were galvanostatically charged and discharged in a current density range of 0.1 C within the voltage range of 0.01–3 V. For the high rate testing, the charge/discharge current gradually increased from 0.1 C to 0.2, 0.5, 1, 2, 5 and 10 C, and then decreased to 1 C and 0.1 C, step by step. Cyclic voltammetry (CV) curves were collected using an electrochemistry workstation (CHI618D) at 0.5 mV s^{-1} in the 0.0-3.0 V range.

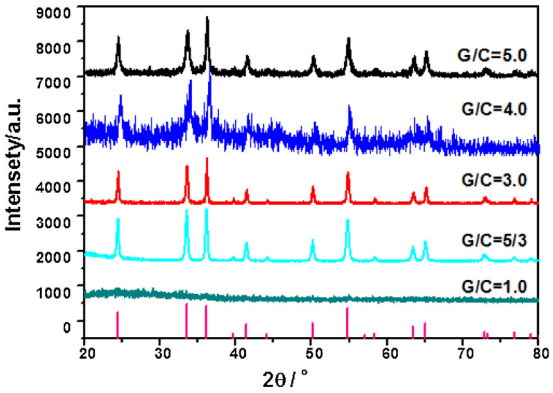

Fig. 1. The XRD patterns of the products obtained by the solution combustion synthesis with different ratio of glycine to chromium nitrate.

3. Results and discussion

3.1. Morphology and structure of Cr_2O_3 nanopaticles

In solution combustion synthesis, the fuel to oxidizer ratio has been previously shown to alter the combustion behavior [33], oxidation state [34,35], morphology and grain size of the products [36,37]. In this work, glycine is used as a fuel. It not only reacts with oxidizer to form a combustion, but also acts as complexing agents reacting with chromium cations, preventing selective precipitation at the heating stage [38]. Therefore, the effect of glycine fuel to chromium nitrate oxidizer ratio (G/C) on the formation of products is investigated in details. Fig. 1 shows the X-ray diffraction (XRD) patterns of the products at different G/C ratios. It is evident that no obvious Bragg diffraction peaks have been detected in the product with G/C = 1, indicating that the product is amorphous. For other products, except for G/C = 1, the obvious diffraction peaks identified for the planes of the Cr_2O_3 crystalline structure can be clearly detected. In solution combustion synthesis, the chemical energy released from the redox exothermic reaction transforms the metal ions to the corresponding metal oxide, and the fuel to oxidizer ratio has an effect on the energy and the oxidation state [39]. For the combustion reaction system in this work, the G/C of 5/3 is stoichiometric, which is predicted by the propellant chemistry criterion. When the G/C is equal to 1, it is a fuel-lean condition. The amount of fuel (glycine) is not enough, and the energy generated during the combustion reaction is not sufficient for the crystallization of Cr_2O_3. If the G/C exceeds 5/3, it is a fuel-rich condition. The energy generated during combustion reactions of stoichiometric and fuel-rich mixtures is sufficient for the crystallization of Cr_2O_3, and the Cr_2O_3 crystal can be easily obtained directly from the reaction of metal nitrates-glycine without further heating or calcined treatment. The crystalline sizes from the XRD were estimated by the Scherrer's formula, and the results were shown in Table 1.

Fig. 2 shows SEM images of the products at different amounts of glycine. As the amount of glycine increases, the morphology of the as prepared products changes from flocculent to the sheet structure. When the glycine-to-chromium nitrate ratio (G/C) is 1 or 5/3, the products are composed of the flocculent structure (Fig. 2a and b). When the G/C is 3, the product is composed of the flocculent and sheet structure (Fig. 2c). As the G/C is increased to 4 and 5, the products are composed of the sheet structure (Fig. 2d and Fig. 2e).

Table 1
Experimental details on samples obtained at different G/C.

G/C	Surface area ($m^2 g^{-1}$)	type of hysteresis and isotherm	pore diameter (nm)	pore volume (cc/g)	crystallite size by XRD (nm)
1	20	IV	20.3	0.099	-
5/3	26	IV	23.1	0.145	41.0
3	30	IV	25.7	0.190	31.6
4	162	IV	4.4	0.178	19.8
5	140	IV	6.3	0.166	30.0

Nitrogen adsorption/desorption isotherms are measured to determine the specific surface area of the products. As the G/C increased from 1, 5/3, 3, 4 to 5, the SSA of the products are 20 $m^2 g^{-1}$, 26 $m^2 g^{-1}$, 30 $m^2 g^{-1}$, 162 $m^2 g^{-1}$ and 140 $m^2 g^{-1}$, determined by the BET method. However, some researchers have reported that the different amount of fuel could affect the SSA and morphology due to the different amount of gases generated during the reaction, reinforcing the dispersant effect on the product particles [40]. In addition, as shown in Table 1, the SSA increases with the decrease of the crystalline size. The comprehension about the great change for the high SSA of the products from the G/C =3 and G/C = 4 is still under investigation.

The nitrogen adsorption–desorption isotherms of all products show type IV characteristics with H2 type of hysteresis. The type of hysteresis and isotherm, porous volume and pore size of the products at different G/C are shown in Table 1. The nitrogen adsorption–desorption isotherm for the product with G/C = 4, is presented in Fig. 3. The physisorption measurement is essentially type-IV isotherm with H2-type hysteresis loops associated with the capillary and wormhole-like pores [41]. Such hysteresis

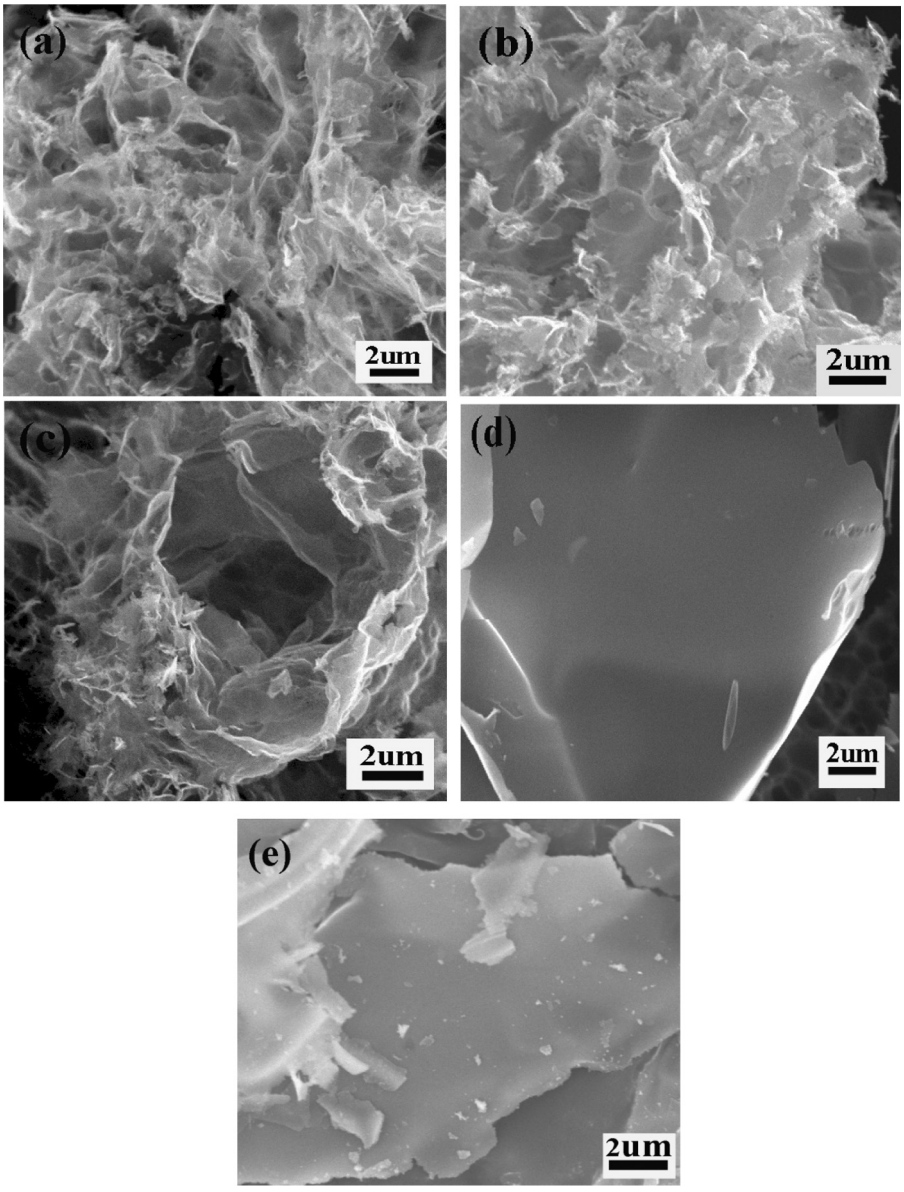

Fig. 2. SEM images of the products obtained by the solution combustion synthesis with different amount of glycine: (a) G/C = 1. (b) G/C = 5/3. (c) G/C = 3. (d) G/C = 4. (e) G/C = 5.

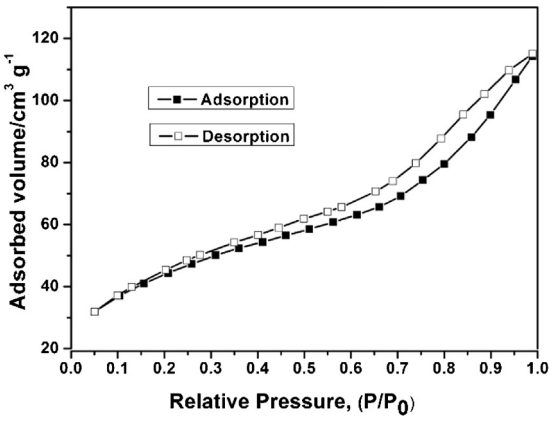

Fig. 3. Nitrogen adsorption/desorption isotherms of the product with G/C =4.

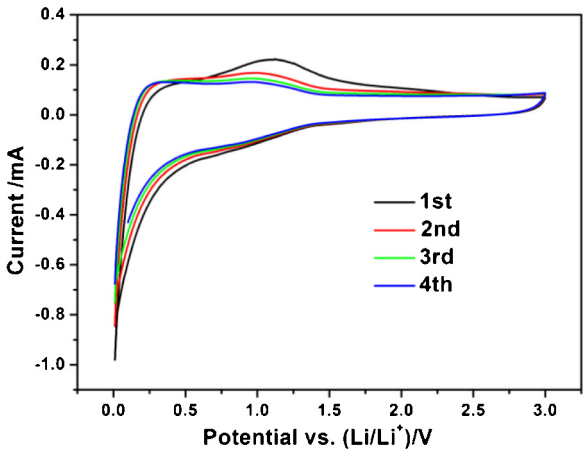

Fig. 5. The first 4 cycles of cyclic voltammetry curves of mesoporous Cr_2O_3 nanoparticles. Scanning rate is 0.5 mV s^{-1} in the 0.01-3 V testing range.

typically indicates the presence of mesopores, according to IUPAC [42]. A large hysteresis loop between the adsorption and desorption isotherms over a P/P_0 range of 0.13–0.98 is the characteristic of highly porous materials, which confirmed the formation of mesopores in the sheet structures. The average pore diameter deduced by adsorption–desorption isotherm is 4.4 nm.

The magnified TEM image of the nanosheet for the product with G/C = 4 is presented in Fig. 4a, which indicates that the sheet structure consists of nanoparticles with a diameter of ~20 nm and the Cr_2O_3 has a porous structure. The particle size is in good agreement with the size obtained by Scherrer formula. From the HRTEM image in Fig. 4b, the fringe of the particle in a Cr_2O_3 corresponds to an interplanar distance of 0.2479 nm. This agrees well with the lattice spacing of the (110) plane of Cr_2O_3.

3.2. Electrochemical performance

Due to the high specific surface area of mesoporous Cr_2O_3 nanopaticles, they are suitable as the LIBs anode materials. The electrochemical properties of the products with G/C = 4 as anode materials for LIBs are investigated. The cyclic voltammetry (CV) profiles of the mesoporous Cr_2O_3 nanopaticles for the initial four cycles are shown in Fig. 5. In the first negative scan of the sample in Fig. 5, one small peak at 0.7 V as well as an obvious peak at 0.01 V are observed. The cathodic peak at 0.7 V is assigned to the irreversible reductive decomposition of the electrolyte forming the SEI layer. This peak decreases in intensity in the 2nd cycle, and completely disappears after the 3rd cycle. This result suggests that the SEI layer is unstable due to the volume change of Cr_2O_3 in the first conversion/deconversion cycle, but stabilizes afterwards. The peak at 0.01 V corresponds to the conversion reaction of Cr_2O_3 with Li. Meanwhile, in the anodic process, a broad peak is present at about 1.08 V, corresponding to the reversible oxidation of Cr^0 to Cr^{3+} [43,44]. In the subsequent cycle, the anodic peak disappears at the second and subsequent cycles. Additionally, peak intensities decrease, which can be attributed to the thermodynamically impossible extraction of Li from Li_2O and the decomposition of electrolyte to form an SEI layer [45].

The charge/discharge curves of the mesoporous Cr_2O_3 nanopaticles for the first four cycles obtained at the current density of 100 mA h g^{-1} in the voltage window of 0.01-3.0 V (vs. Li/Li^+) are presented in Fig. 6. It can be seen that the first and second specific discharge capacity of the mesoporous Cr_2O_3 nanoparticles is as high as 1676 mA h g^{-1} and 1079 mA h g^{-1}, respectively. It is larger than the theoretical capacity of 1058 mA h g^{-1}, which can be due to the SEI (solid electrolyte interphase) layer forming by the decomposed electrolyte at low voltage and further lithium insertion via interfacial charging at the metal/Li_2O interfaces [46,47]. In addition, there is a plateau at 0.7 V only for the initial discharge capacities. It is assigned to the irreversible reductive decomposition of the electrolyte forming the SEI layer. The overlap of the third and the fourth discharge curves shows that the Cr_2O_3 sheet structure electrode is stable during these cycles.

Furthermore, the mesoporous Cr_2O_3 nanoparticles also support the cycle performance, as revealed by Fig. 7. Even after 55 cycles, the reversible capacity of Cr_2O_3 is stable and still retains at 480 mA h g^{-1}. The cycling performance of the mesoporous Cr_2O_3 nanopaticles with varied current rates is revealed in Fig. 8. For the high testing rate, the charge/discharge current gradually increases from 0.1 C to 0.2, 0.5, 1, 2, 5 and 10 C, then decreases to 1 C and 0.1 C, step

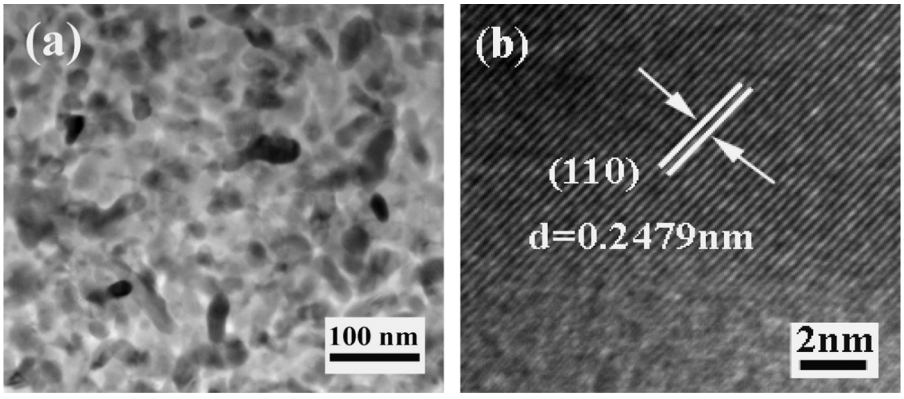

Fig. 4. Characterization of the product with G/C = 4: (a) TEM image. (b) HRTEM image.

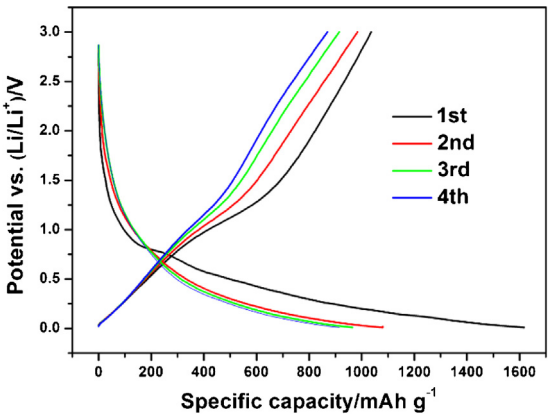

Fig. 6. The first four charge/discharge curves of mesoporous Cr_2O_3 nanoparticles at a current density of 100 mA g^{-1}, in the 0.01-3.0 V voltage range.

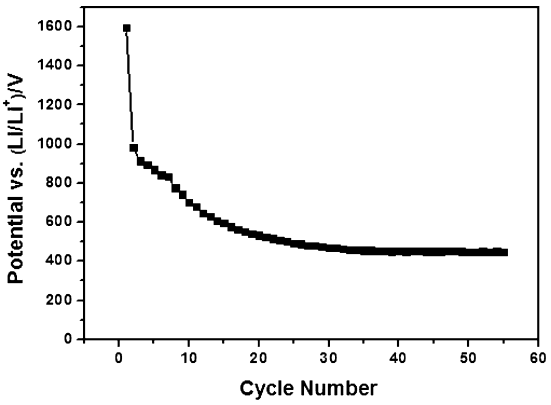

Fig. 7. Cycle performance of mesoporous Cr_2O_3 nanoparticles (at 0.1 C rate).

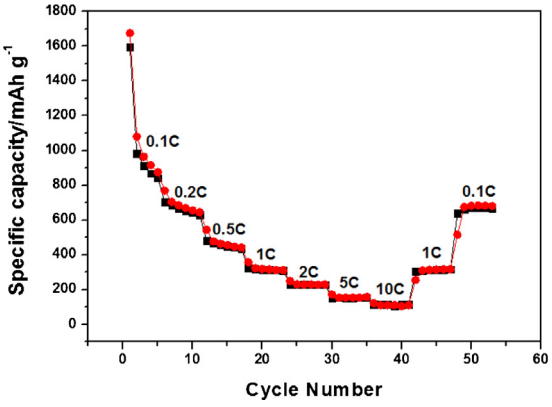

Fig. 8. The rate capabilities of mesoporous Cr_2O_3 nanopaticles by multiple step galvanostatic testing (at rates of 0.1, 0.2, 0.5, 1, 2, 5, 10 C, and then return to the 1 and 0.1 C step by step).

by step. The capacity decreases at the 0.1 C and 0.2 steps, ascribed to the active material undergoing minor structural rearrangement and making good electrical contact with the conducting carbon particles in the composite electrode, the current-collector and the liquid electrolyte. After 10 cycles, the capacity is stable at the same current rate. A decrease in capacity value is observed at higher rates. After 48 cycles, the current rate is reduced from 10 C to 1 C and 0.1 C, and still a reversible capacity of 684 mA h g^{-1} is obtained. This shows the good rate capability of the material.As a result, the high surface area and morph The large surface area of Cr_2O_3 offers more actives sites for the electronic and ionic transport. The feature of mesoporous Cr_2O_3 with high surface-to-volume ratio is its nanosize crystalline walls. The lithium ions insertion/extraction to the thinner crystal walls can complete faster and provides enough structural stability for the electrode, culminating in its good cycling stability. ological characteristics of mesoporous Cr_2O_3 enhance the transport of Li^+ ions and electrons within the composite electrode and surface incorporation of Li^+ into the electrochemically active particles, achieving enhanced rate capability.

4. Conclusions

In summary, this work demonstrates the successful synthesis of mesoporous Cr_2O_3 with a high specific surface area of 162 m^2 g^{-1} by the solution combustion method. The mesoporous Cr_2O_3 has a sheet structure, which consists of nanoparticles with an average size of 20 nm. The as-prepared mesoporous Cr_2O_3 nanoparticles exhibit enhanced performance for lithium ion batteries, which is mainly due to the high surface area and morphological characteristics of mesoporous materials. This study clearly indicates the synthesis of high performance anode material by simple solution combustion synthesis and this technique can be extended for other transition metal oxides used in the development of high power lithium-ion batteries.

Acknowledgements

This work is supported by the National Natural Science Foundation Program of China (50802006) and (51172017), the Program for the New Century Excellent Talents in University (NCET-10-0226), and the Fundamental Research Funds for the Central Universities (FRF-TP-11-004A) and the National 863 Program.

References

[1] L. Ji, O. Toprakci, M. Alcoutlabi, Y. Yao, Y. Li, S. Zhang, B. Guo, Z. Lin, X. Zhang, ACS Appl. Mater. Interfaces 4 (2012) 2672–2679.
[2] M. Armand, J.M. Tarascon, Nature 451 (2008) 652–657.
[3] J.M. Tarascon, M. Armand, Nature 414 (2001) 359–367.
[4] A.S. Arico, P. Bruce, B. Scrosati, J.M. Tarascon, W.V. Schalkwijk, Nat. Mater. 4 (2005) 366–377.
[5] P.G. Bruce, B. Scrosati, J.M. Tarascon, Angew. Chem. Int. Ed. 47 (2008) 2930–2946.
[6] C.T. Cherian, J. Sundaramurthy, M. Kalaivani, P. Ragupathy, P.S. Kumar, V. Thavasi, J. Mater. Chem. 22 (2012) 12198–12204.
[7] P.L. Taberna, S. Mitra, P. Poizot, P. Simon, J.M. Tarascon, J. M. Nat. Mater. 5 (2006) 567–573.
[8] K.T. Nam, D.W. Kim, P.J. Yoo, C.Y. Chiang, N. Meethong, P.T. Hammond, Y.M. Chiang, A.M. Belcher, Science 321 (2006) 885–888.
[9] D. Qian, B. Xu, H.-M. Cho, T. Hatsukade, K.J. Carroll, Y.S. Meng, Chem. Mater 24 (2012) 2744–2751.
[10] E. Hosono, S. Fujihara, I. Honma, H.S. Zhou, Electrochem. Commun. 8 (2006) 284–288.
[11] P.C. Wang, H.P. Ding, T. Bark, C.H. Chen, Electrochim. Acta 52 (2007) 6650–6655.
[12] N. Rudawski, B. Darby, B. Yates, A.A. Volinsky, K.S. Jones, Appl. Phys. Lett. 100 (9) (2012) 083111.
[13] N.G. Rudawski, B.R. Yates, M.R. Holzworth, K.S. Jones, R.G. Elliman, A.A. Volinsky, J. Power Sources 223 (2013) 336–340.
[14] P. Poizot, S. Laruelle, S. Grugeon, L. Dupont, J.M. Tarascon, Nature 407 (2000) 496–499.
[15] P. Poizot, S. Laruelle, S. Grugeon, L. Dupont, J.M. Tarascon, J. Power Sources 97–98 (2001) 235–239.
[16] J. Cabana, L. Monconduit, D. Larcher, M.R. Palac, Adv. Mater. 22 (2010) E170–E192.
[17] M.V. Reddy, S. Madhavi, S.G.V. Rao, B.V.R. Chowdari, J. Power Sources 162 (2006) 1312–1321.
[18] M.V. Reddy, S. Madhavi, S.G.V. Rao, B.V.R. Chowdari, Chem. Rev. 113 (2013) 5364–5457.
[19] J. Hu, H. Li, X.J. Huang, J. Electrochem. Solid-State Lett. 8 (2005) A66–A69.
[20] S. Grugeon, S. Laruelle, L. Dupont, F. Chevallier, P.L. Taberna, P. Simon, L. Gireaud, S. Lascaud, E. Vidal, B. Yrieix, J.M. Tarascon, Chem. Mater. 17 (2005) 5041–5047.
[21] H. Li, P. Balaya, J. Maier, J. Electrochem. Soc. 151 (2004) A1878–A1885.
[22] L. Dupont, S. Laruelle, S. Grugeon, C. Dickinson, W. Zhou, J.M. Tarascon, J. Power Sources 175 (2008) 502–509.
[23] L. Dupont, S. Grugeon, S. Laruelle, J.M. Tarascon, J. Power Sources 164 (2007) 839–848.

[24] H. Liu, X. Du, X. Xing, G. Wang, S.Z. Qiao, Chem. Commun. 48 (2012) 865–867.
[25] I. Tamiolakis, I.N. Lykakis, A.P. Katsoulidis, M. Stratakis, G.S. Armatas, Chem. Mater. 23 (2011) 4204–4211.
[26] C. Dickinson, W.Z. Zhou, R.P. Hodgkin, Y.F. Shi, D.Y. Zhao, H.Y. He, Chem. Mater. 18 (2006) 3088–3095.
[27] A.S. Prakash, P. Manikandan, K. Ramesha, M. Sathiya, J.-M. Tarascon, A.K. Shukla, Chem. Mater. 22 (2010) 2857–2863.
[28] P.A. Deshpande, S. Polisetti, G. Madras, Langmuir 27 (2011) 3578–3587.
[29] M. Mapa, C.S. Gopinath, Chem. Mater. 21 (2009) 351–359.
[30] S.T. Aruna, N.S. Kini, N.S. Rajam, Mater. Res. Bull. 44 (2009) 728–733.
[31] J. Bai, J. Liu, C. Li, G. Li, D. Du, Adv. Powder Technol. 22 (2011) 72–76.
[32] A. Chu, M. Qin, Rafi-ud-din, B. Jia, H. Lu, X. Qu, J. Am. Ceram. Soc 95 (2012) 2510–2515.
[33] K. Deshpande, A. Mukasyan, A. Varma, Chem. Mater. 16 (2004) 4896.
[34] C.-H. Jung, S. Jalota, S.B. Bhaduri, Mater. Lett. 59 (2005) 2426.
[35] S.S. Manoharan, P. Swati, J. Sigamani, M.L. Rao, R.K. Sahu, J. Am. Ceram. Soc. 85 (2002) 2469.
[36] P. Erri, J. Nader, A. Varma, Adv. Mater. 20 (2008) 1243–1245.
[37] B. Zhao, X. Yu, R. Cai, R. Ran, H. Wang, Z. Shao, J. Mater. Chem. 22 (2012) 2900–2907.
[38] S.R. Nair, R.D. Purohit, A.K. Tyagi, P.K. Sinha, B.P. Sharma, Mater. Res. Bull. 43 (2008) 1573–1582.
[39] D.A. Fumo, M.R. Morelli, A.M. Segadaes, Mater. Res. Bull. 31 (1996) 1243–1255.
[40] A. Chu, M. Qin, Rafi-ud-dina, B. Jia, H. Lu, X. Qu, J. Alloys Compd 530 (2012) 144–151.
[41] B.Y. Yu, S.-Y. Kwak, J. Mater. Chem. 22 (2012) 8345–8353.
[42] S. Lowell, J.E., Shields, M.A., Thomas, M., Thommes, M. Kluwer Academic Publishers, Boston, 4th edn 2004, 101–126.
[43] J.-T. Li, V. Maurice, J. Swiatowska-Mrowiecka, A. Seyeux, S. Zanna, L. Klein, S.-G. Sun, P. Marcus, Electrochim. Acta 54 (2009) 3700–3707.
[44] J. Hu, H. Li, X. Huang, L. Chen, Solid State Ionics 177 (2006) 2791–2799.
[45] J. Chen, L.N. Xu, W.Y. Li, X.L. Gou, Adv. Mater. 17 (2005) 582–586.
[46] P. Balaya, H. Li, L. Kienle, J. Maier, Adv. Funct. Mater. 13 (2003) 621–625.
[47] J. Jamnik, J. Maier, Phys. Chem. Chem. Phys. 5 (2003) 5215–5220.